Published in final edited form as:
Neuroimage. 2013 July 1; 74: 288–297. doi:10.1016/j.neuroimage.2013.02.035.

Infraslow LFP correlates to resting-state fMRI BOLD signals

Wen-Ju Pan[1], **Garth John Thompson**[1], **Matthew Evan Magnuson**[1], **Dieter Jaeger**[2], and **Shella Keilholz**[1,*]

[1]Department of Biomedical Engineering, Emory University/Georgia Institute of Technology

[2]Department of Biology, Emory University

Abstract

The slow fluctuations of the blood-oxygenation-level dependent (BOLD) signal in resting-state fMRI are widely utilized as a surrogate marker of ongoing neural activity. Spontaneous neural activity includes a broad range of frequencies, from infraslow (< 0.5 Hz) fluctuations to fast action potentials. Recent studies have demonstrated a correlative relationship between the BOLD fluctuations and power modulations of the local field potential (LFP), particularly in the gamma band. However, the relationship between the BOLD signal and the infraslow components of the LFP, which are directly comparable in frequency to the BOLD fluctuations, has not been directly investigated. Here we report a first examination of the temporal relation between the resting-state BOLD signal and infraslow LFPs using simultaneous fMRI and full-band LFP recording in rat. The spontaneous BOLD signal at the recording sites exhibited significant localized correlation with the infraslow LFP signals as well as with the slow power modulations of higher-frequency LFPs (1–100 Hz) at a delay comparable to the hemodynamic response time under anesthesia. Infraslow electrical activity has been postulated to play a role in attentional processes, and the findings reported here suggest that infraslow LFP coordination may share a mechanism with the large-scale BOLD-based networks previously implicated in task performance, providing new insight into the mechanisms contributing to the resting state fMRI signal.

Introduction

Resting-state fMRI is widely employed to investigate functional connectivity and the activity of large-scale networks in the brain (Biswal et al., 1995; Fox and Raichle, 2007). The spontaneous low-frequency fluctuations (< 0.1 Hz) in the blood-oxygen-level dependent (BOLD) signal have been postulated to reflect variations in neural activity over time. Researchers investigating the neural substrate of resting-state fMRI have reported a correlational relationship between the spontaneous BOLD fluctuations and slow fluctuations of the band-limited power (BLP) of the local field potential (LFP) in the well-recognized frequency bands from delta to gamma (Magri et al., 2012; Pan et al., 2011; Shmuel and Leopold, 2008). It has been suggested that the infraslow components of electrophysiological recordings (below 0.5 Hz) also play a functional role in the coordination of large-scale networks (Birbaumer et al., 1990; He et al., 2008; Khader et al., 2008), but their relationship to the BOLD fluctuations in the resting state is largely unknown. The infraslow fluctuations

*Corresponding author. Address: 101 Woodruff Circle WMB 2001, Atlanta, GA 30322; Phone: 404-727-2433; Fax: 404-727-9873; shella.keilholz@bme.gatech.edu.

have traditionally been discarded due to concerns about contamination from drift and non-neural variation, but more recently this frequency range has received increasing attention as a growing body of research demonstrates its relevance to cognitive processing (Khader et al., 2008). For example, Rosler et al. demonstrated that a larger amplitude of a slow wave pattern was linked to more specific modular resources of cognition, which seems to reflect a connection between slow wave amplitude and how strongly a particular cell assembly is activated at a given time (Rosler et al., 1997). DC-EEG studies have linked infraslow activity to fluctuations in attentional control and reaction time in both normal subjects and attention deficit/hyperactivity disorder (ADHD) patients (Helps et al.; Monto et al., 2008). Infraslow fluctuations of negative shifts may represent increased cortical excitability because of widespread depolarization in the dendritic trees of cortical pyramidal neurons, thereby facilitating the processing of stimuli presented to a more easily excitable network (Elbert, 1993; Rockstroh et al., 1993).

The frequency correspondence between the infraslow electrical activity and the spontaneous BOLD signal has led several groups to postulate a direct link between the two (Drew et al., 2008; He et al., 2008). In support of a relationship between infraslow electrophysiological signals and BOLD fluctuations, He et al. compared the correlation structures of the sensorimotor network via fMRI and electrocorticography (ECoG) separately on the same group of epilepsy patients and demonstrated largely similar topography in the correlation patterns whether revealed by spontaneous slow BOLD signals or by spontaneous slow cortical potentials (He et al., 2008), suggesting the two are closely linked. However, to obtain the temporal relationship between the BOLD signal and infraslow neural activity, technically-challenging simultaneous fMRI and direct current (DC) recording experiments are essential. To date, previous simultaneous fMRI and intracortical recording were limited to conventional LFP bands (> 0.5 Hz) (Goense and Logothetis, 2008; Logothetis et al., 2001; Pan et al., 2011; Shmuel and Leopold, 2008). We have recently developed an animal model of simultaneous fMRI and electrophysiology using micro-glass Ag/AgCl electrodes implanted in the rat brain (Pan et al., 2010b; Pan et al., 2011). The slowly varying components in electrophysiology can be more faithfully recorded with chloridized silver than with other kinds of electrodes (Tallgren et al., 2005). Full-band local field potentials were recorded from somatosensory cortex (S1FL, $n = 13$) and the caudate putamen (CP, $n = 3$) while fMRI was acquired simultaneously from the same slice. The low frequency BOLD fluctuations were compared to the simultaneously-recorded infraslow LFPs to examine spatial co-localization and the temporal relationship between the signals. To partially account for potentially confounding effects of anesthesia on the vasculature, two anesthetics with different effects on neural activity and the vasculature (isoflurane (ISO) group, $n = 6$ rats; dexmedetomidine (DMED) group, $n = 7$ rats) were compared in S1FL data.

Our results demonstrate that the spontaneous BOLD signals at the recording sites exhibited significant correlation with the infraslow LFP fluctuations as well as power modulation of traditional LFPs at a delay comparable to the hemodynamic response time in stimulation studies. Highly localized correlation was also observed in the homologous cortical area in the opposite hemisphere, demonstrating a close correlational relationship between spontaneous fluctuations in the infraslow potentials and BOLD signals and suggesting that coherent infraslow fluctuations may play an important role in functional connectivity.

Materials and Methods

Animal preparation and electrode implantation

All animal experiments were performed in compliance with NIH guidelines and were approved by the Emory University Institutional Animal Care and Use Committee. Sprague-Dawley rats (male, 200 – 300 g, $n = 16$, Charles River) were used in this study. All rats were

anesthetized with 2% isoflurane during surgery. A fine tip electrode (~10 μm in diameter, borosilicate pipettes) with 1 – 5 MΩ was prepared with a micropipette puller (PE-2; NARISHIGE). The electrode was filled with artificial cerebrospinal fluid (ACSF), which served as conductive media bridging the chloridized silver wire to the extracellular environment. The details of the surgical procedures and microelectrode implantation have been described elsewhere (Pan et al., 2010b; Pan et al., 2011). To summarize, a pair of micro-glass electrodes were implanted in S1FL of the left and right hemispheres separately and secured to the skull for most rats ($n = 13$). An additional 3 rats were implanted with glass electrodes in the caudate putamen (CP) of the right hemisphere. The key step in the animal preparation is to place and secure the microelectrodes with minimal impact on fMRI image quality. We identified several ways that surgery could cause EPI artifacts and employed corresponding strategies to mitigate the potential problems. First, the skin and muscle tissue above the skull were removed for craniotomy, which resulted in an artifact in the brain image due to the susceptibility difference between the brain and the air. In practice, a layer of paste (Colgate, NY), which has a T2 similar to brain tissue, was applied to replace the removed skin and muscle over the skull. The paste replacement helped to reduce the MRI susceptibility mismatch near the brain surface. Secondly, the implanted pipettes must be secured to the skull bone by dental cement (methyl methacrylate); the latter has no MR signal and may cause similar MRI susceptibility artifacts along the brain surface. To avoid this, instead of applying cement on the bone near the pipette tip, which would fall within the imaging slice, the cement was used just at the area > 0.5 mm posterior to the imaging slice (neighboring the lambdoid suture). The pipette was placed at a 45 degree angle to the brain surface and secured via cement to the middle of the pipette shaft. Another merit of this oblique placement is that only the electrode tips are present in the imaging slice, which avoids unwanted signal from the high water content of the solution in the shaft of the pipette. The sharp tip contains a small amount of solution and has a minimal impact on EPI quality. In the primary group, a pair of micropipettes was implanted into the middle of the cortex (0.5–1 mm below cortical surface) at bilateral primary somatosensory areas separately (S1FL, 4 mm lateral and 1 mm frontal to bregma). In the CP group, one micropipette was implanted into the middle of the CP (2.5 mm below cortical surface) in the right hemisphere (2 mm lateral and 1 mm frontal to bregma). In addition, we examined the effect of implantation depth using single site dual-electrode implantation and simultaneous fMRI. To make the dual glass electrodes, the tips of the two micropipettes were closely placed together under a microscope and one was bent at a small angle by heating, keeping a 1-mm difference in tip ends, and the shafts of the pair were glued together with dental cement. The dual-electrode was implanted in S1FL, one in the deep cortex (>1mm below cortical surface) and another in the superficial cortex (just dipped into the cortex under the microscope). The chloridized silver wire dipped into the electrolyte of the pipette served as an electrode transferring field potential variations to the amplifier via a twisted-pair cable. A chloridized silver wire was placed under the skin caudal to the incision over the skull to serve as a reference/ground. The recording cables were ~5 meters long (the amplifiers are located outside the magnet room; A–M Systems, model 3000) and were covered with conductive plastic, which served as a passive shield. Detailed procedures for the surgery and electrode implantation are available as a video from the Journal of Visualized Experiments (Pan et al., 2010b) and are also described elsewhere (Pan et al., 2011).

Simultaneous fMRI and DC recording

All imaging was performed on a 9.4 T/30 cm horizontal bore small animal MRI system (Bruker, Billerica, MA). A three-plane scout image was first acquired to position the fMRI scans. To improve the homogeneity of the magnetic field, the volume of interest (6 mm^3) was shimmed using FASTMAP (Gruetter, 1993). Manual shimming adjustment was then applied when necessary to improve the field homogeneity of the selected slice. For fMRI

studies, a coronal imaging slice was selected to cover bilateral S1FL and CP areas, in which the glass recording electrode tips were implanted. The EPI imaging parameters were FOV, 1.92 × 1.92 cm^2; matrix size, 64 × 64; in-plane resolution, 0.3 × 0.3mm^2; slice thickness, 2mm; TR/TE, 500/15 ms. Resting-state scans were collected under ~1.5% isoflurane (ISO, n = 6; electrodes in S1FL) or dexmedetomidine (DMED, n = 7 for S1FL electrodes; n = 3 for CP electrodes) anesthesia. The isoflurane, in a mixture of 70% O_2 and 30% room air, was continuously delivered to the nosecone, allowing for free breathing throughout the experiment. The rat's oxygen saturation, measured with a pulse oximeter, was kept above 98% throughout the data acquisition process. For DMED studies, a bolus of 0.025 mg/kg dexmedetomidine was injected subcutaneously. Isoflurane was disconnected 10 min afterwards, and switched to a continuous subcutaneous infusion of dexmedetomidine (0.05 mg/kg/h). The dose was increased by a factor of three (0.15 mg/kg/h) after ~1.5 hr, following the protocol for prolonged sedation described in (Pawela et al., 2009). The DMED scans were conducted > 3 hr after switching from ISO to avoid any residual ISO effects (Pan et al., 2010a). The simultaneous fMRI and recording for each session lasted 10 min for DC recording (which began 1 min prior to image acquisition and continued after acquisition was complete) and 8 min for fMRI (1000 single-slice images per scan). Twenty dummy scans were acquired to reduce transient signal intensity fluctuations at the start of the image series. The recording parameters were as follows: × 500 amplified, 0 – 100 Hz bandpass-filtered, 60 Hz notch-filtered, and 12 kHz sampling rate for analog to digital conversion using a 16 bit analog-to-digital converter (PCI-6281; National Instruments). All physiological parameters were monitored and maintained within normal ranges, including rectal temperature, respiration rate, SpO_2/cardiac rate. The animals were sacrificed at the end of the experiment.

fMRI data preprocessing

Data were analyzed using MatLab (Mathworks) and SPM 8 (www.fil.ion.ucl.ac.uk/spm). The brain mask for each individual rat was calculated by a Region Growing method from a seed pixel in the brain area of the selected slice. The region is iteratively grown by comparing all unallocated neighboring pixels to the region. The difference between a pixel's intensity value and the region's mean is used as a measure of similarity. The pixel with the smallest difference measured this way is allocated to the region. This process stops when the intensity difference between the region mean and the new pixel becomes larger than a certain threshold. The EPI signal intensity in the rat brain is generally greater than the adjacent pixel signal intensity outside brain, which allows detection of the brain region by this method. In the image matrix, two or more rows/columns outside the brain mask were removed to decrease image size and the time needed to process the data set. Head motion occurring during scanning sessions was corrected in SPM using the cropped image matrix. If the brain position shifted more than one pixel across the data acquisition period or if "spike-like" abrupt head motion was observed, the data were not used for further analysis. The images were then smoothed using a Gaussian filter with an FWHM of 0.5 mm in all directions (0.3 × 0.3 mm^2 in-plane pixel resolution). Linear drift and global signals were removed by regression. Finally, the time series of each voxel in the brain area of the selected slice was normalized to unit variance (percent change) and bandpass-filtered (0.01 – 0.1 Hz for ISO data, 0.01 – 0.25 Hz for DMED data; based on previous work demonstrating contributions from higher frequencies in the DMED rats (Magnuson et al., 2010; Williams et al., 2010) before correlation analysis.

Electrophysiological data preprocessing

The raw signals recorded during simultaneous fMRI scanning contained a combination of neural signals and artifacts, such as periodic noise due to EPI acquisition. These imaging-related artifacts were removed offline in Matlab (Mathworks), as illustrated elsewhere (Pan

et al., 2011). A TTL signal from the MRI system indicated the beginning of each EPI scan and was used to identify each scan epoch in the electrical recording time course. A template of the noise structure due to EPI acquisition was obtained by averaging all TR periods together and then subtracted from each time course (Allen et al., 2000). Example raw LFP traces (after gradient noise removal) for ISO and DMED are shown in Fig. S1. These LFPs were band-pass filtered (0.01 – 0.1 Hz for ISO data, 0.01 – 0.25 Hz for DMED data) for further correlation analysis with fMRI data. The time courses were re-sampled to the same temporal resolution as fMRI data using negative mean value of each scan epoch (TR, 0.5 sec) as a new time course. Because the electrodes were positioned in the depth (~0.5 mm below surface) of the cortex where the burst direction appears as a negative shift, the infraslow field potentials were sign-reversed before further correlation or coherence analysis with the BOLD signal. The band-limited power (BLP) for each frequency range was calculated by fast Fourier transform as described elsewhere (Pan et al., 2011).

Correlation analysis of fMRI and infraslow LFP signals

The infraslow LFP time course for each recording site, S1FL or CP, was used as a "seed" to conduct Pearson correlation with the BOLD time course of each voxel of the imaged brain slice using varying BOLD lags (−9.5 sec to 9.5 sec in 0.5 sec increments). All the statistical analyses were performed in MatLab. The Pearson correlation r_{xy} was estimated between x_i and y_i where $i = 1,2, \ldots, n$ (n is total pixels within the imaged brain slice), according to the formula

$$r_{xy} = \frac{n\sum x_i y_i - n\sum x_i \sum y_i}{\sqrt{n\sum x_i^2 - (\sum x_i)^2}\sqrt{n\sum y_i^2 - (\sum y_i)^2}}$$

FDR corrections for multiple comparison (Genovese et al., 2002) at $p < 0.05$ were conducted to evaluate significant correlation across all voxels and the 25 different time lags.

Coherence analysis of fMRI and LFP signals

For further examination of the frequencies involved in the BOLD/infraslow LFP correlation, the BOLD time course of the voxel with the maximum correlation at the recording site was extracted and the time lag to maximal correlation was removed to temporally align the BOLD and LFP signal. The un-filtered time courses were used to perform BOLD/infraslow LFP coherence analysis, and the coefficient of each frequency between 0 and 1 Hz was calculated. Additionally, as a control, time-reversed infraslow LFPs were used for the same coherence analysis. The simultaneous recording included high frequency components up to 100 Hz as well as infraslow components. The band-limited power (BLP) was calculated from LFP bands with a time bin of 2000 ms for 1 – 4 Hz LFP, 1000 ms for 4 – 8 Hz and 500 ms for > 8 Hz signals. All BLP time series were obtained at steps of 500 ms, which results in the same temporal resolution as the BOLD signal. Several frequency bands, including 1 – 4 Hz, 4 – 8 Hz, 8 – 14 Hz, 14 – 25 Hz, 25 – 40 Hz and 40 – 100 Hz, were converted to BLP time series (Pan et al., 2011). The coherence for each frequency from 0 to 1 Hz between BOLD and each BLP was calculated for each rat under ISO ($n = 6$) or DMED ($n = 7$). Mathematically, the coherence (C_{xy}) for a given pair of time series, BOLD/infraslow LFP or BOLD/BLP, was estimated as the magnitude squared of the input signals x and y using Welch's averaged, modified periodogram method. The magnitude squared coherence estimate is a function of frequency with values between 0 and 1 that indicates how well x corresponds to y at each frequency. The coherence is a function of the power spectral density (P_{xx} and P_{yy}) of x and y and the cross power spectral density (P_{xy}) of x and y

$$Cxy(f)=\frac{|Pxy(f)|^2}{Pxx(f)Pyy(f)}$$

Results

Tight local coupling between infraslow LFP and BOLD signals

Robust BOLD/infraslow LFP correlations were observed in rats under both isoflurane (ISO, Fig. 1A) and dexmedetomidine (DMED, Fig. 1B) anesthesia. In both groups of rats, our data showed that the strongest correlation between infraslow LFP and BOLD occurs in voxels near the recording electrode in S1FL of the recording hemisphere (Fig. 1A and B), with contralateral S1FL also exhibiting relatively high correlation. As expected, the pattern of correlation with the BOLD signal is highly similar when either the left or the right electrode is used (Fig. S2), indicating that the infraslow LFPs are correlated with each other as well as with the BOLD fluctuations. Spatially, the extent of the significantly correlated region varies in different anesthetic states, being relatively widespread in ISO (Fig. 1B1) relative to DMED (Fig. 1B2). Similar patterns of BOLD/infraslow LFP correlation were found in the CP recording data (Fig. 2). As a control, simultaneous DC recordings and BOLD measurements were acquired from a dead rat using identical methods, and no significant correlation was detected (Fig. S3). In addition, the dual-electrode recordings (superficial vs. deep) in S1FL (Fig. S4) show that the BOLD signal in S1FL is strongly correlated with infraslow LFP signals from both depths, though the direction of the electrical signal is inverted in deep vs. superficial layers. In the primary group of animals, all electrical signals were recorded in deep cortex (>0.5 mm below the cortical surface), so we inverted the infraslow LFP signal direction to be consistent with the BOLD signal.

The findings provide direct evidence of a temporal correlation between the fMRI signal and infraslow LFP in the resting state. The significantly correlated regions are mostly in functionally associated anatomical areas, i.e. bilateral somatosensory cortex when recording from S1FL, or bilateral CP when recording from CP. The network patterns are in agreement with the recent report by He et al. (He et al., 2008) and the BOLD/infraslow LFP coupling suggests that coherent infraslow activity may mediate coordination within a functional network commonly observed in fMRI.

Time-lagged BOLD relative to infraslow LFP

To empirically account for the hemodynamic response time, the BOLD time course was shifted relative to the infraslow LFP time course in 0.5 sec increments (TR = 0.5 sec, from −9.5 sec to 9.5 sec). The BOLD/infraslow LFP correlation coefficients were measured from voxels near the recording electrode and plotted as a function of time shift (Fig. 1B). Peak correlation occurred when BOLD lagged infraslow LFP by 4 sec in the ISO group (Fig. 1 A1 and B1) and by 2.5 sec in the DMED group (Fig. 1 A2 and B2). The lag time for the CP recording experiments under DMED was identical to the lag time for the cortical areas. These time lags are similar to hemodynamic response times measured in the rat, and the 4-sec lag of BOLD to infraslow LFP is identical to the lag between BOLD and LFPs (not including the infraslow frequencies) reported in our recent simultaneous fMRI/conventional LFP recordings in the rat under ISO (Pan et al., 2011). A 4-sec BOLD lag in response to stimulation has also been reported in the rat under Urethane anesthesia (Martin et al., 2006). Interestingly, when a light anesthesia, DMED, is used, the BOLD latency is shorter, ~ 2.5 sec (Fig. 1 A2 and B2), which approaches the hemodynamic delay (2 sec) observed by Martin et al. in the awake rat (Martin et al., 2006). Consistent with previous studies using simultaneous imaging and recording of conventional higher frequency LFPs, no significant

correlation was observed when the BOLD signal preceded the electrical signal or when a long lag time separated the DC recording and the BOLD data (Fig. 1). Interestingly, the positive correlation in the ISO group begins to rise at negative time points and remains positive for the entire range of times examined. One possible interpretation may be the different filtering properties of neurovascular coupling in different anesthetic states, i.e. slow in ISO and fast in DMED. The slow BOLD response to the spontaneous neural activities under ISO might blur the correlation in our measures.

The BOLD data was band pass filtered between 0.01 to 0.1 Hz for ISO and 0.01 to 0.25 Hz for DMED, based on previous studies showing that the frequency content of BOLD is higher for DMED (Majeed et al., 2009; Williams et al., 2010). To ensure that the changes in the time delay between infraslow LFP and maximally correlated BOLD were not due to the use of different filters for the two anesthetic groups, the same frequency ranges (0.01–0.25 Hz) were examined for both anesthesia groups. When a frequency range of 0.01–0.25 Hz (corresponding to the range used for DMED) was used for the ISO group instead of the original range of 0.01–0.1 Hz, no significant change in lag time to peak correlation occurred (maximum correlation: 3.58 ± 0.08 vs. 3.92 ± 0.52 sec respectively, paired *t*-test, $p = 0.54$).

BOLD/infraslow LFP coherence

One potentially important issue is to define the frequency range in the BOLD fluctuations that is coupled with the neural signal. Ongoing extracellular potentials can span a broad range of frequencies, from arbitrarily slow changes to fast action potentials, but the BOLD signal fluctuations in resting-state functional networks are typically on the scale of 10 sec to 100 sec (Biswal et al., 1995). In which frequency ranges are the hemodynamic signals consistent with the cortical field potentials? To address this issue, coherence analysis was used to examine the contribution of each individual frequency for infraslow potentials and BOLD signals containing all frequency components between 0 and 1 Hz. The unfiltered BOLD time courses were acquired from the voxel exhibiting the maximal correlation with infraslow potentials at the recording site. The time-lagged BOLD time course (at peak correlation with infraslow potentials) was then used for further frequency coherence analysis with electrical recordings. As a control analysis, coherence was also calculated between time-reversed potential signals and the BOLD time courses. The group average results showed that peaks of high coherence were centered near 0.1 Hz in the ISO data (Fig. 3A) and between 0.1 – 0.2 Hz in the DMED data (Fig. 3B), in line with previous findings based on the BOLD power spectra alone (Majeed et al., 2009; Williams et al., 2010). The frequency specific BOLD/infraslow LFP coherence was not found in the control group (Fig. 3, gray plot) and significant differences in peak coherences between real data and control existed. The results of coherence analysis are consistent with the correlation results when averaging signals over a frequency range. For example, the range of low frequencies in each anesthetic condition was compared with a control from the neighboring frequency range (indicated by a bracket in Fig. 3, 0.2–0.3 Hz in ISO or 0.25–0.5 Hz in DMED) when calculating BOLD/infraslow LFP correlations. The low frequencies produced higher correlation with spatial localization in the somatosensory cortex, while the control frequencies did not exhibit localized correlation (Fig. 3). Regardless of the spectral variations due to the anesthesia effects, the strong BOLD/infraslow LFP coherence and correlation were present and limited to the low frequencies.

BOLD/BLP coherence

The raw recordings included very slow field potentials and the higher frequencies of conventional LFPs (see methods). Therefore additional coherence analysis between BOLD and the band-limited power (BLP) of the LFP (> 1 Hz) was conducted as well. The BLP exhibits slow variations in LFP power, which allows direct comparison with the slow BOLD

signals during spontaneous activity (Leopold et al., 2003). The average coherence of each frequency component from all rats of each anesthesia groups is plotted in Fig. 4. Relative to the higher frequencies, the frequencies below 0.1 Hz in ISO data (Fig. 4A1) or below 0.25 Hz in DMED data (Fig. 4B1) exhibited higher BOLD/BLP coherences. Lower frequency BLP bands (delta and theta) were more coherent with BOLD than higher frequency BLP bands (beta and gamma) in the DMED rats ($p = 0.035$, paired t-test), while the ISO rats exhibited broadband coherence in the low frequencies. The results are in agreement with our recent findings, which used traditional AC amplifiers and examined only the conventional LFP frequencies (> 1 Hz) (Pan et al., 2011). Similar to the coherence between BOLD and infraslow LFPs, the coherence between BOLD and BLP in the ISO rats is limited to a narrow range of low frequencies, while the BOLD/BLP coherence for the DMED rats is wider and contains slightly higher frequency components. As a control analysis, coherence was also calculated between time-reversed BOLD time courses and BLPs (Fig. 4 A2 and B2), showing significant differences from the real data at the peak frequencies (averaging all BLP bands, $p < 0.05$, paired t-test).

For comparison between BOLD coupling with infraslow LFP and with BLP, we examined the coherence difference between the two using a paired t-test (Fig. 5). The difference was always positive, but only significant for alpha and gamma bands of BLP in the DMED group.

Discussion

The wide disparities in time scale make it challenging to establish a direct relationship between slow BOLD fluctuations and the well-recognized faster neural oscillations in electrophysiology. These fast electrophysiological frequencies (> 0.5 Hz) cannot be captured directly by BOLD due to the low-pass filter inherent in the vasculature (Logothetis and Wandell, 2004). Most researchers have chosen to calculate band-limited power for time bins corresponding to the sampling interval between BOLD images (Pan et al., 2011; Schölvinck et al., 2010; Shmuel and Leopold, 2008), an approach that has provided valuable insight into the relationship between neural activity and spontaneous BOLD fluctuations. Apart from these well-recognized LFP components, however, there are more tonic components in recording, the infraslow waves, which have received less attention. These slow neural changes are potentially compatible in time scale with the slow BOLD fluctuations that occur in spontaneous activity, and are postulated to coordinate activity between large-scale brain regions (Monto et al., 2008; Steriade, 2001), making them excellent candidates for the neural basis of BOLD functional connectivity (Drew et al., 2008). The neural infra-slow signal has been a controversial issue in historical electrophysiological studies, but recent studies have demonstrated that slow cortical potentials are more likely of neural origination rather than merely artificial drifts (He and Raichle, 2009; Monto et al., 2008; Rosler et al., 1997; Trimmel et al., 1990). No meaningful correlations between infraslow electrical variations and fMRI were found during simultaneous recording and imaging in a dead rat (Fig. S3), supporting a physiological origin for the signal correlation. If, as our study suggests, infraslow LFP and BOLD fluctuations share a common mechanism, MRI studies of functional connectivity and network interactions with their noninvasive, whole brain coverage may provide insight into the spatial and temporal properties of the physiological infra-slow fluctuations from a neural complex. At the same time, the coupling between infraslow LFP and BOLD provides direct and important insight into the slow electric signaling basis of spontaneous fMRI signal and may aid in the interpretation of human studies.

Temporal correlation

The present study provided a direct examination of the temporal relation between fMRI BOLD and infraslow LFP in the rat brain and demonstrated a close temporal relationship between them. The direct coupling of these signals suggests a common mechanism behind the spontaneous fluctuations in extracellular field potential and local blood oxygenation. Despite different time lags under different anesthetics (DMED, 2.5 sec; ISO, 4 sec), BOLD signals were consistently delayed relative to infraslow LFP changes. The time-lagged correlations in BOLD to infraslow LFP suggest possible causality as BOLD follows infraslow LFP events.

It is interesting to note that negative correlations are often observed at longer time lags, particularly in the data acquired under dexmedetomidine. Negative correlation between areas has been widely observed in BOLD studies (Fox et al., 2005), but in this case, the finding is positive correlation at one time lag and negative correlation at another, all within the same area. We believe that some fraction of these infraslow potentials may actually be organized in spatiotemporal patterns across the whole brain. Our previous work has demonstrated spatiotemporal patterns in the BOLD signal from both rats and humans that appear to have a quasi-periodic structure (Majeed et al., 2011; Majeed et al., 2009). The negative correlation is then a function of the periodicity of the signal As seen in the dexmedetomidine data (Fig. 1 B2), the relationship between BOLD and infraslow potentials ranges from positive to negative as a function of lag time, and a suggestion of propagation from lateral to medial areas is present. The spatial and temporal aspects of these patterns match well with the quasi-periodic fluctuations detected in BOLD alone (Majeed et al., 2011). Anticorrelations between LFP power have also been observed in recording studies and may have a similar basis (Popa et al., 2009).

The negative correlations were not observed in the data acquired under ISO. It is possible that the cycle is prolonged under ISO, as the time to peak is longer under ISO than under DMED (4 vs 2.5 s). However, for the pattern of positive and negative correlations to match the scale of the DMED pattern (positive peak at 2.5s, negative peak at 5–5.5 s), the negative peak would be expected at 8–10 s, suggesting that a trend toward negavitivity would be evident in the last time points shown in Figure 1. This is not the case, and no pattern of negative correlation at long delay times was observed in our preliminary analysis of BOLD/LFP correlation in individual rats which used a larger range of lag times. We speculate that the difference may be due to the vasoactive properties of the two anesthetics. The vasodilation induced by ISO may bias the vasculature towards lower frequencies and blur the response to electrical activity. More work will be needed to unravel the relative contributions of the neural and vascular effects of the anesthetic agents.

Spatial pattern

Our voxelwise correlation analysis revealed a spatially-localized pattern of correlation between BOLD and infraslow LFP. It is important to note that the correlation exhibited spatial patterns localized within functional systems, rather global correlation across the brain. The findings from anesthetized animals have been compared to sleep in humans, where slow waves are an important phenomenon. These waves are often considered a global phenomenon, but recent research has shown that these slow waves actually exist on a continuum of levels from low amplitude local waves to strong global waves (Nir et al., 2011). This finding makes it more plausible that these fluctuations are linked to fMRI signals, which commonly present as patterned regional connectivity in a functional system instead of global fluctuations (He and Raichle, 2009). The long-distant correlation patterns imply a potential common network mechanism shared by BOLD and infraslow LFP signals

and are in agreement with the notion that slow cortical activities play an essential role in large-scale brain network mechanisms (Lu et al., 2007; Steriade, 2001).

It is possible for global signal removal during preprocessing to induce artificial anticorrelation (Gavrilescu et al., 2002; Murphy et al., 2009). However in our analyses, the BOLD/infraslow correlations were robust with or without global signal regression. The BOLD time lag and spatial pattern are similar for both cases (Fig. S2). It has been shown that at least part of the global BOLD signal can be linked to a neural origin (Schölvinck et al., 2010). More recently, reports suggested that the global cortical LFP activity in the rat may be modulated by respiration (Roy et al., 2012). However, regardless of the origin of the global signal, it does not appear to be a major contributor to the correlation between infraslow LFPs and BOLD in functional somatosensory networks.

Frequency coupling and anesthesia effects

The most significant frequencies in the BOLD fluctuations and functional connectivity are slow components, below 0.1 Hz in human resting state studies. In contrast, neural oscillations contain a much broader range of frequencies, which can temporally coexist in the same or different structures and interact with each other in mammalian cortex (Steriade, 2001). Both the coherent frequencies of the BOLD/infraslow LFP fluctuations and the time delay between the infraslow signal and the maximally correlated BOLD signal were affected by the choice of anesthetic. In our data analysis, different frequency ranges were used for filtering the BOLD signal from rats under ISO and DMED, raising the possibility that filter effects may contribute to the observed differences in the time delay to maximum correlation between BOLD and the infraslow LFPs. However, a subsequent analysis that applied the broader filter used for DMED to the ISO group did not find a significant change in the time delay for that group.

One possibility is that the variations in lag time arise from the effects of the anesthetic on the vascular tone. ISO and DMED have inverse effects on the vasculature, with ISO causing vasodilation and DMED causing vasoconstriction (Ohata et al., 1999). The vascular smooth muscle under ISO may become relaxed and reduce the vessel's ability to pulsate quickly; on the contrary, the vessel wall under DMED could become tighter, facilitating higher frequency pulsation. Another, more intriguing possibility is that the frequencies and time delay are actually governed by the activity of the astrocytic syncytium. Poskanzer et al. showed that astrocytes can trigger UP states in vivo (Poskanzer and Yuste, 2011), and Schummers et al. demonstrated that astrocytes can be activated by very specific stimuli, with their calcium release delayed by a few seconds relative to that of nearby neurons (Schummers et al., 2008). The delay was comparable to the "hemodynamic" delays observed in this study, i.e. ~4 sec delay under isoflurane. If the delay between neuronal and astrocytic activity is the major contributor to the time lag between the electrical recordings and the BOLD response, DMED may somehow facilitate astrocyte calcium release upon neuronal activity, a topic for future investigations. It is known that different anesthetics alter the baseline energy consumption and neural signaling of the brain, and that these changes are linked to differences in the neural and BOLD responses to sensory stimulation (Maandag et al., 2007). Similar baseline effects on the relationship between BOLD and neural activity in the absence of stimulation are certainly plausible.

In support of an astrocytic source for the time lag, infraslow LFPs have recently been linked to both calcium waves and local changes in blood flow (Kuga et al., 2011). The calcium waves were dependent on neural activity and blocked by tetrodotoxin. These studies suggest that infraslow LFPs and the BOLD signal fluctuations arise from a complex interaction between neurons, astrocytes, and the vasculature that cannot be disentangled with our existing data. To quantify the contributions of different origins, independent measures of

blood flow or metabolism or even neural firing rates will be valuable additions to future work.

While the frequency range of the hemodynamic fluctuations varies under different anesthetics, the BOLD/infraslow LFP coupling is largely preserved in our results. It is particularly interesting to note that previous studies in animal models report discrepancies in the frequency ranges that are most closely linked to the BOLD signal when calculating correlation between BOLD and field potentials, including gamma band (Shmuel and Leopold, 2008), alpha to gamma (Magri et al., 2012) or delta to gamma (Pan et al., 2011). These studies were performed under different anesthetics. From the data shown in Fig. 3, it appears that different anesthetics alter the coherence between BLPs and the BOLD signal, which may account for the variation in previous reports. The relative delay between BOLD and LFP may also be dependent on species, as reports from monkey studies find a lag time of 3.5–6 seconds (Magri et al., 2012; Murayama et al., 2010; Shmuel and Leopold, 2008). Similar variations in the hemodynamic delay are also observed in stimulation-based studies (Logothetis et al., 2001). Meanwhile, our work suggests that full-band electrophysiological recordings, including infraslow signals, should be obtained and examined in combined fMRI/electrophysiology studies of spontaneous brain function, since both fast and slow field potentials may contribute to BOLD signal, as demonstrated here.

Possible infraslow LFP origins

The mechanism underlying infraslow LFP generation is not fully understood, though it has been suggested that slow cortical potentials reflect cortical modulation of neuronal excitability (Rockstroh et al., 1993; Rosler et al., 1997). For example, recent studies have indicated that slow neural signals might play an important role in the neural signaling of large-scale networks (Birbaumer et al., 1990; He et al., 2008; Khader et al., 2008). The synaptic activity at apical dendrites in superficial layers has been proposed as the main factor contributing to the slow cortical potentials, demonstrated by simultaneous multiple layer recordings across cortex (Mitzdorf, 1985). The long-lasting excitatory postsynaptic potentials at these apical dendrites may be measured from superficial or deep layers, but the two signals are inverse (He and Raichle, 2009). The depth recordings in our study exhibit mostly downward electrical bursting for all subjects. The infraslow fluctuations appear to follow the same direction as the high frequency LFPs, i.e. downward bursting in depth recording. The inverse signal directions between superficial and depth recordings were examined with simultaneously dual-electrode recording and fMRI, demonstrated in Fig. S4. As expected, both superficial and depth recorded infraslow LFP signals correlate to fMRI signals in roughly the same cortical region (Fig. S4), which suggests the infraslow potentials share the same neural origin as the LFPs, mainly from apical dendrites (He and Raichle, 2009). As discussed in the context of the time delay between infraslow activity and the BOLD signal, there are indications that the infraslow cortical potentials are generated by the coordinated action of the neuronal and glial networks (Fellin et al., 2009; Schummers et al., 2008) and are associated with local changes in blood flow, a plausible mechanism linking infraslow LFPs and MRI signal changes. It should be noted that much of the work on the origin of slow cortical potentials was performed in the context of the slow waves that occur during sleep, and there is reason to believe that the infraslow potentials described in this study (typically an order of magnitude slower than slow waves) are not necessarily the same and may, in fact, modulate the slow waves (He et al., 2008).

Potential significance and future directions

Recent work has indicated that infraslow fluctuations play a role in attention (Helps et al., 2010; Monto et al., 2008). A similar link to attention and performance has been found for two networks widely studied using resting state BOLD and functional connectivity mapping

(Fox et al., 2007; Kelly and Garavan, 2005; Thompson et al., 2012). The default mode network (DMN) and task positive network (TPN)(Fox et al., 2005) are large cortical networks that are typically anticorrelated with each other. Because the infraslow fluctuations are tightly linked to the BOLD signal as shown in our data, the common link to attentional control leads us to speculate that the DMN and TPN observed with BOLD may reflect underlying patterns of infraslow activity. An additional piece of support comes from previous work showing that reproducible spatiotemporal patterns of BOLD signal involving areas of the DMN and TPN can be observed in human subjects (Majeed et al., 2011). Similar patterns were detected in rats anesthetized with DMED and the timing and propagation pattern of the BOLD signal is similar to the timing of the positive and negative correlations observed between infraslow fluctuations and BOLD. These findings hint that the infraslow fluctuations may have a quasi-periodic spatiotemporal organization that organizes the networks observed in BOLD functional connectivity studies. If this is true, it may be possible to map the infraslow activity throughout the brain with unprecedented resolution using the BOLD signal as a surrogate, a step that would impact research into attentional disorders.

The variation in the extent and timing of the coupling between BOLD and infraslow activity as a function of the baseline brain state also highlights the importance of understanding and characterizing the spontaneous activity of the brain prior to interpretation of functional connectivity measures. While most studies in humans involve unanesthetized subjects, a variety of factors cause the brain's baseline blood flow and metabolism to vary even within an individual. For example, caffeine decreases functional connectivity and the amplitude of global fluctuations (Wong et al., NeuroImage 2012). These findings emphasize the importance of quantitatively characterizing the baseline state of the brain, , a challenging endeavour in human subjects.

While the relationship between spontaneous infraslow LFP fluctuations and the more recognized high-frequency components of LFP signals needs to be fully characterized, both appear to contribute to the BOLD signal via neurovascular coupling. One working model in neuroscience considers brain organization to occur in a nested manner, with high frequencies coordinating local activity and low frequencies mediating long-range interactions. This study and other experiments that use combined imaging and recording have found relationships between the BOLD signal and electrical frequencies from infraslow all the way to gamma, suggesting that the BOLD signal may reflect contributions from local activity as well as large scale fluctuations. The spontaneous BOLD fluctuations then contain a wealth of information about slow and fast field potentials in the cortex and will undoubtedly prove a valuable tool for deciphering normal and disordered brain function.

Supplementary Material

Refer to Web version on PubMed Central for supplementary material.

Acknowledgments

Funding sources: NIH, 1R21NS072810-01A1 and 1R21NS057718-01

References

Allen PJ, Josephs O, Turner R. A method for removing imaging artifact from continuous EEG recorded during functional MRI. Neuroimage. 2000; 12:230–239. [PubMed: 10913328]

Birbaumer N, Elbert T, Canavan AG, Rockstroh B. Slow potentials of the cerebral cortex and behavior. Physiol Rev. 1990; 70:1–41. [PubMed: 2404287]

Biswal B, Yetkin FZ, Haughton VM, Hyde JS. Functional connectivity in the motor cortex of resting human brain using echo-planar MRI. Magn Reson Med. 1995; 34:537–541. [PubMed: 8524021]

Drew PJ, Duyn JH, Golanov E, Kleinfeld D. Finding coherence in spontaneous oscillations. Nat Neurosci. 2008; 11:991–993. [PubMed: 18725901]

Elbert, T. Slow cortical potentials reflect the regulation of cortical excitability. In: McCallum, WC., editor. Slow Potential Changes of the Human Brain. New York: Plenum; 1993. p. 235-251.1993

Fellin T, Halassa MM, Terunuma M, Succol F, Takano H, Frank M, Moss SJ, Haydon PG. Endogenous nonneuronal modulators of synaptic transmission control cortical slow oscillations in vivo. Proc Natl Acad Sci U S A. 2009; 106:15037–15042. [PubMed: 19706442]

Fox MD, Raichle ME. Spontaneous fluctuations in brain activity observed with functional magnetic resonance imaging. Nat Rev Neurosci. 2007; 8:700–711. [PubMed: 17704812]

Fox MD, Snyder AZ, Vincent JL, Corbetta M, Van Essen DC, Raichle ME. The human brain is intrinsically organized into dynamic, anticorrelated functional networks. Proc Natl Acad Sci U S A. 2005; 102:9673–9678. [PubMed: 15976020]

Fox MD, Snyder AZ, Vincent JL, Raichle ME. Intrinsic fluctuations within cortical systems account for intertrial variability in human behavior. Neuron. 2007; 56:171–184. [PubMed: 17920023]

Gavrilescu M, Shaw ME, Stuart GW, Eckersley P, Svalbe ID, Egan GF. Simulation of the effects of global normalization procedures in functional MRI. Neuroimage. 2002; 17:532–542. [PubMed: 12377132]

Genovese CR, Lazar NA, Nichols T. Thresholding of statistical maps in functional neuroimaging using the false discovery rate. Neuroimage. 2002; 15:870–878. [PubMed: 11906227]

Goense JB, Logothetis NK. Neurophysiology of the BOLD fMRI signal in awake monkeys. Curr Biol. 2008; 18:631–640. [PubMed: 18439825]

Gruetter R. Automatic, localized in vivo adjustment of all first- and second-order shim coils. Magn Reson Med. 1993; 29:804–811. [PubMed: 8350724]

He BJ, Raichle ME. The fMRI signal, slow cortical potential and consciousness. Trends Cogn Sci. 2009; 13:302–309. [PubMed: 19535283]

He BJ, Snyder AZ, Zempel JM, Smyth MD, Raichle ME. Electrophysiological correlates of the brain's intrinsic large-scale functional architecture. Proc Natl Acad Sci U S A. 2008; 105:16039–16044. [PubMed: 18843113]

Helps SK, Broyd SJ, James CJ, Karl A, Chen W, Sonuga-Barke EJ. Altered spontaneous low frequency brain activity in attention deficit/hyperactivity disorder. Brain Res. 1322:134–143. [PubMed: 20117101]

Helps SK, Broyd SJ, James CJ, Karl A, Chen W, Sonuga-Barke EJS. Altered spontaneous low frequency brain activity in Attention Deficit/Hyperactivity Disorder. Brain Res Brain Res Rev. 2010; 1322:134–143.

Kelly AM, Garavan H. Human functional neuroimaging of brain changes associated with practice. Cereb Cortex. 2005; 15:1089–1102. [PubMed: 15616134]

Khader P, Schicke T, Roder B, Rosler F. On the relationship between slow cortical potentials and BOLD signal changes in humans. Int J Psychophysiol. 2008; 67:252–261. [PubMed: 17669531]

Kuga N, Sasaki T, Takahara Y, Matsuki N, Ikegaya Y. Large-scale calcium waves traveling through astrocytic networks in vivo. J Neurosci. 2011; 31:2607–2614. [PubMed: 21325528]

Leopold DA, Murayama Y, Logothetis NK. Very slow activity fluctuations in monkey visual cortex: implications for functional brain imaging. Cereb Cortex. 2003; 13:422–433. [PubMed: 12631571]

Logothetis NK, Pauls J, Augath M, Trinath T, Oeltermann A. Neurophysiological investigation of the basis of the fMRI signal. Nature. 2001; 412:150–157. [PubMed: 11449264]

Logothetis NK, Wandell BA. Interpreting the BOLD signal. Annu Rev Physiol. 2004; 66:735–769. [PubMed: 14977420]

Lu H, Zuo Y, Gu H, Waltz JA, Zhan W, Scholl CA, Rea W, Yang Y, Stein EA. Synchronized delta oscillations correlate with the resting-state functional MRI signal. Proc Natl Acad Sci U S A. 2007; 104:18265–18269. [PubMed: 17991778]

Maandag NJ, Coman D, Sanganahalli BG, Herman P, Smith AJ, Blumenfeld H, Shulman RG, Hyder F. Energetics of neuronal signaling and fMRI activity. Proc Natl Acad Sci U S A. 2007; 104:20546–20551. [PubMed: 18079290]

Magnuson M, Majeed W, Keilholz SD. Functional connectivity in blood oxygenation leveldependent and cerebral blood volume-weighted resting state functional magnetic resonance imaging in the rat brain. J Magn Reson Imaging. 2010; 32:584–592. [PubMed: 20815055]

Magri C, Schridde U, Murayama Y, Panzeri S, Logothetis NK. The Amplitude and Timing of the BOLD Signal Reflects the Relationship between Local Field Potential Power at Different Frequencies. J Neurosci. 2012; 32:1395–1407. [PubMed: 22279224]

Majeed W, Magnuson M, Hasenkamp W, Schwarb H, Schumacher EH, Barsalou L, Keilholz SD. Spatiotemporal dynamics of low frequency BOLD fluctuations in rats and humans. Neuroimage. 2011; 54:1140–1150. [PubMed: 20728554]

Majeed W, Magnuson M, Keilholz SD. Spatiotemporal dynamics of low frequency fluctuations in BOLD fMRI of the rat. J Magn Reson Imaging. 2009; 30:384–393. [PubMed: 19629982]

Martin C, Martindale J, Berwick J, Mayhew J. Investigating neural-hemodynamic coupling and the hemodynamic response function in the awake rat. Neuroimage. 2006; 32:33–48. [PubMed: 16725349]

Mitzdorf U. Current source-density method and application in cat cerebral cortex: investigation of evoked potentials and EEG phenomena. Physiol Rev. 1985; 65:37–100. [PubMed: 3880898]

Monto S, Palva S, Voipio J, Palva JM. Very slow EEG fluctuations predict the dynamics of stimulus detection and oscillation amplitudes in humans. J Neurosci. 2008; 28:8268–8272. [PubMed: 18701689]

Murayama Y, Biessmann F, Meinecke FC, Muller KR, Augath M, Oeltermann A, Logothetis NK. Relationship between neural and hemodynamic signals during spontaneous activity studied with temporal kernel CCA. Magn Reson Imaging. 2010; 28:1095–1103. [PubMed: 20096530]

Murphy K, Birn RM, Handwerker DA, Jones TB, Bandettini PA. The impact of global signal regression on resting state correlations: are anti-correlated networks introduced? Neuroimage. 2009; 44:893–905. [PubMed: 18976716]

Nir Y, Staba RJ, Andrillon T, Vyazovskiy VV, Cirelli C, Fried I, Tononi G. Regional slow waves and spindles in human sleep. Neuron. 2011; 70:153–169. [PubMed: 21482364]

Ohata H, Iida H, Dohi S, Watanabe Y. Intravenous dexmedetomidine inhibits cerebrovascular dilation induced by isoflurane and sevoflurane in dogs. Anesth Analg. 1999; 89:370–377. [PubMed: 10439750]

Pan, W-J.; Magnuson, M.; Thompson, G.; Jaeger, D.; Keilholz, S. Tight Coupling of Resting-state BOLD Fluctuations with Intracortical DC Changes in Rat Somatosensory Cortex during Prolonged Medetomidine Sedation. ISMRM 19th Scientific Meeting & Exhibition; Montreal, Canada. 2010a. (#949)

Pan W-J, Thompson G, Magnuson M, Majeed W, Jaeger D, Keilholz S. Simultaneous FMRI and electrophysiology in the rodent brain. J Vis Exp. 2010b

Pan W-J, Thompson G, Magnuson M, Majeed W, Jaeger D, Keilholz S. Broadband Local Field Potentials Correlate with Spontaneous Fluctuations in Functional Magnetic Resonance Imaging Signals in the Rat Somatosensory Cortex Under Isoflurane Anesthesia. Brain Connectivity. 2011; 1:119–131. [PubMed: 22433008]

Pawela CP, Biswal BB, Hudetz AG, Schulte ML, Li R, Jones SR, Cho YR, Matloub HS, Hyde JS. A protocol for use of medetomidine anesthesia in rats for extended studies using taskinduced BOLD contrast and resting-state functional connectivity. Neuroimage. 2009; 46:1137–1147. [PubMed: 19285560]

Popa D, Popescu AT, Pare D. Contrasting activity profile of two distributed cortical networks as a function of attentional demands. J Neurosci. 2009; 29:1191–1201. [PubMed: 19176827]

Poskanzer KE, Yuste R. Astrocytic regulation of cortical UP states. Proc Natl Acad Sci U S A. 2011; 108:18453–18458. [PubMed: 22027012]

Rockstroh B, Muller M, Wagner M, Cohen R, Elbert T. "Probing" the nature of the CNV. Electroencephalogr Clin Neurophysiol. 1993; 87:235–241. [PubMed: 7691554]

Rosler F, Heil M, Roder B. Slow negative brain potentials as reflections of specific modular resources of cognition. Biol Psychol. 1997; 45:109–141. [PubMed: 9083647]

Roy, S.; Ito, J.; Cao, Y.; Gruen, S.; Heck, DH. Delta/theta band LFP oscillations and gamma band power in mouse barrel cortex are coupled to respiratory rhythm Society for Neuroscience. New Orleans: 2012.

Schummers J, Yu H, Sur M. Tuned responses of astrocytes and their influence on hemodynamic signals in the visual cortex. Science. 2008; 320:1638–1643. [PubMed: 18566287]

Schölvinck ML, Maier A, Ye FQ, Duyn JH, Leopold DA. Neural basis of global resting-state fMRI activity. Proc Natl Acad Sci U S A. 2010

Shmuel A, Leopold DA. Neuronal correlates of spontaneous fluctuations in fMRI signals in monkey visual cortex: Implications for functional connectivity at rest. Hum Brain Mapp. 2008; 29:751–761. [PubMed: 18465799]

Steriade M. Impact of network activities on neuronal properties in corticothalamic systems. J Neurophysiol. 2001; 86:1–39. [PubMed: 11431485]

Tallgren P, Vanhatalo S, Kaila K, Voipio J. Evaluation of commercially available electrodes and gels for recording of slow EEG potentials. Clinical Neurophysiology. 2005; 116:799–806. [PubMed: 15792889]

Thompson GJ, Magnuson ME, Merritt MD, Schwarb H, Pan WJ, McKinley A, Tripp LD, Schumacher EH, Keilholz SD. Short-time windows of correlation between large-scale functional brain networks predict vigilance intraindividually and interindividually. Hum Brain Mapp. 2012 (in press).

Trimmel M, Mikowitsch A, Groll-Knapp E, Haider M. Occurrence of infraslow potential oscillations in relation to task, ability to concentrate and intelligence. Int J Psychophysiol. 1990; 9:167–170. [PubMed: 2228750]

Williams KA, Magnuson M, Majeed W, LaConte SM, Peltier SJ, Hu X, Keilholz SD. Comparison of alpha-chloralose, medetomidine and isoflurane anesthesia for functional connectivity mapping in the rat. Magn Reson Imaging. 2010; 28:995–1003. [PubMed: 20456892]

Wong CW, Olafsson V, Tal O, Liu TT. Anti-correlated networks, global signal regression, and the effects of caffeine in resting-state functional MRI. NeuroImage. 2012; 63(1):356–364. [PubMed: 22743194]

Highlights

1. First simultaneous fMRI and infraslow LFP recordings in rat brain
2. Temporal correlation between infraslow LFP and resting state BOLD fluctuations
3. Correlation localized to cortex near electrode and contralateral hemisphere
4. Relationship was present under two different anesthetics

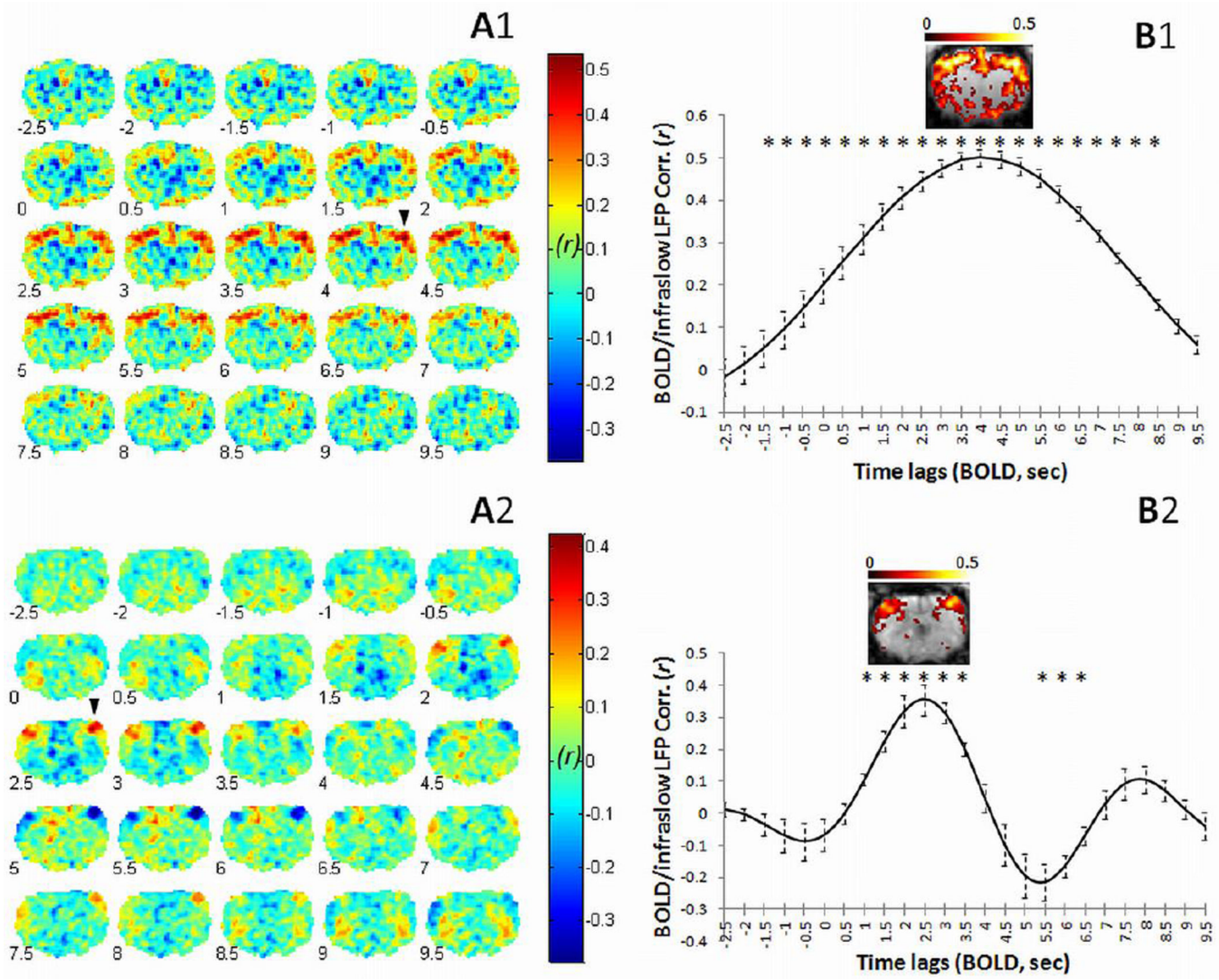

Fig. 1.

Time-lagged correlation between BOLD and infraslow LFP during spontaneous activity. Correlation was calculated between infraslow LFPs (< 0.1 Hz in ISO; < 0.25 Hz in DMED), left or right hemisphere at S1FL, and BOLD (< 0.1 Hz in ISO; < 0.25 Hz in DMED) signals from each voxel in the imaged slice of the brain. The results for the two anesthetic groups are shown separately in the top row (under ISO) and the bottom row (under DMED). Time-lagged correlation maps of representative results are shown on the left, with average ROI results from all rats on the right. The arrow head indicates the ROI of the recording site, which exhibits the highest correlation between infraslow LFP and BOLD at 4 sec lag under ISO (A1 and A2) and 2.5 sec lag under DMED (A2 and B2). The hemisphere opposite the recording site also shows high BOLD/infraslow LFP correlation. The number at the left bottom corner of each brain represents the BOLD time lag (sec). The average correlation values (mean ± SEM) are plotted against time lag on the right column (B1, ISO, $n = 6$ rats; B2, DMED, $n = 7$ rats), showing BOLD/infraslow LFP correlation as a function of time lag. The stars indicate significant differences from the mean value of the first two points ($p < 0.05$, paired t-test on z values, $z=0.5*\ln((1+r)/(1-r))$, corrected for multiple comparisons). The significant BOLD/infraslow LFP correlation (FDR corrected, $p < 0.05$) at the peak time

lag for each group is shown in warm colors (B1 and B2). The left side of the brain is on the left side of the image. Color bar values represent Pearson *r*.

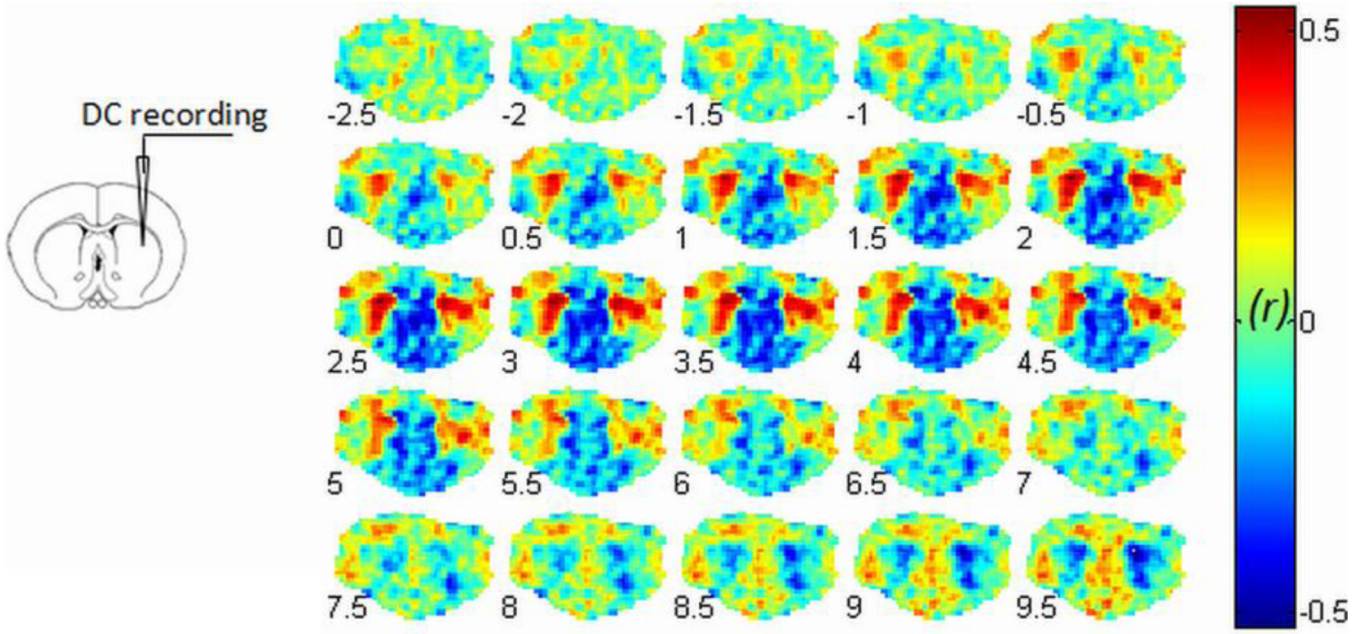

Fig. 2.

Simultaneous DC recording from CP during fMRI. The recording site in the caudate putamen (CP) is illustrated at left panel. The BOLD/infraslow LFP correlation results with varied BOLD lags (−2.5 sec to 9.5 sec) are shown in the right panel. The maximum correlation is observed in bilateral CP when the BOLD signal is delayed by 2.5 sec relative to infraslow LFP under dexmedetomidine. The left side of the brain is on the left side of the image.

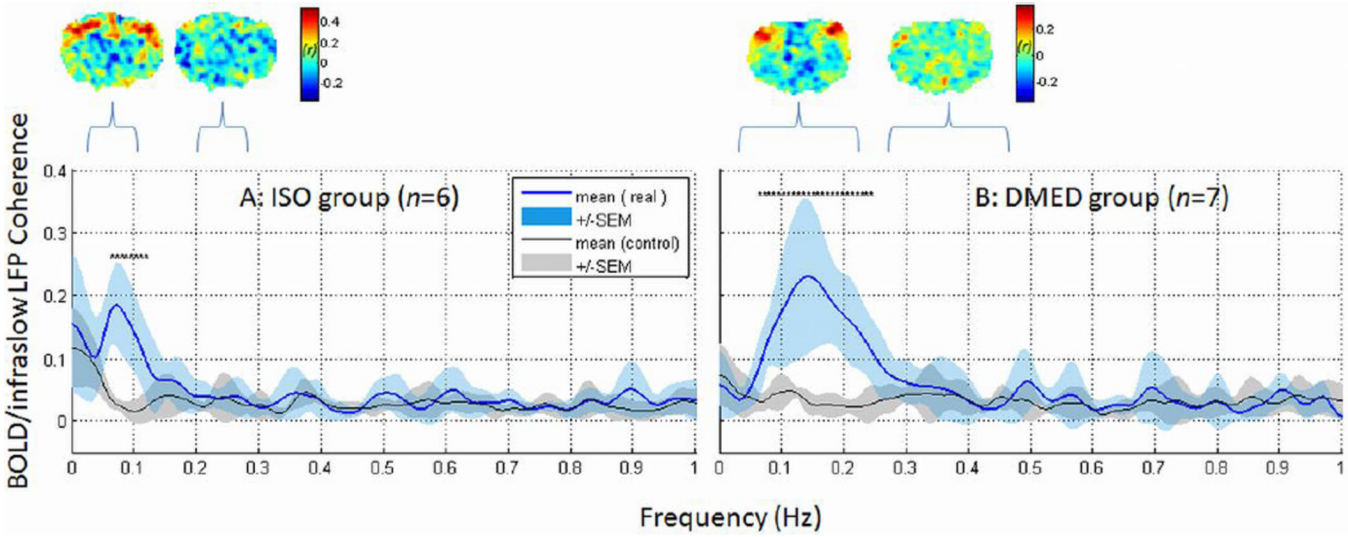

Fig. 3.

Frequency contribution to BOLD/infraslow LFP coupling. Coherence analysis showed high BOLD/infraslow LFP coherence in the low frequencies (blue, mean ± SEM), peaking below 0.1 Hz in ISO anesthesia (A) and below 0.25 Hz in DMED (B). The same analysis was performed with time-reversed infraslow LFP signals as a control. The BOLD/time-reversed infraslow LFP coherence for each frequency is plotted in gray (mean ± SEM). The significant difference ($p < 0.05$, corrected) between the coherences of real data and the control are indicated with a star (*). All significant differences are around coherence peak frequencies. To estimate the frequency contribution to BOLD/infraslow LFP correlation, the low frequency range was compared with the neighboring higher frequency range (indicated by a bracket, 0.2–0.3 Hz in ISO or 0.25–0.5 Hz in DMED). Examples of BOLD/infraslow LFP correlation from a representative rat for each range are shown above the coherence plot. Notably, strong BOLD/infraslow LFP correlation at the recording site was observed with the signals filtered in the low frequency ranges (< 0.1 Hz in ISO or < 0.25 Hz in DMED, indicated with brackets), but not the nearby higher frequencies (0.2–0.3 Hz in ISO or 0.25–0.5 Hz in DMED).

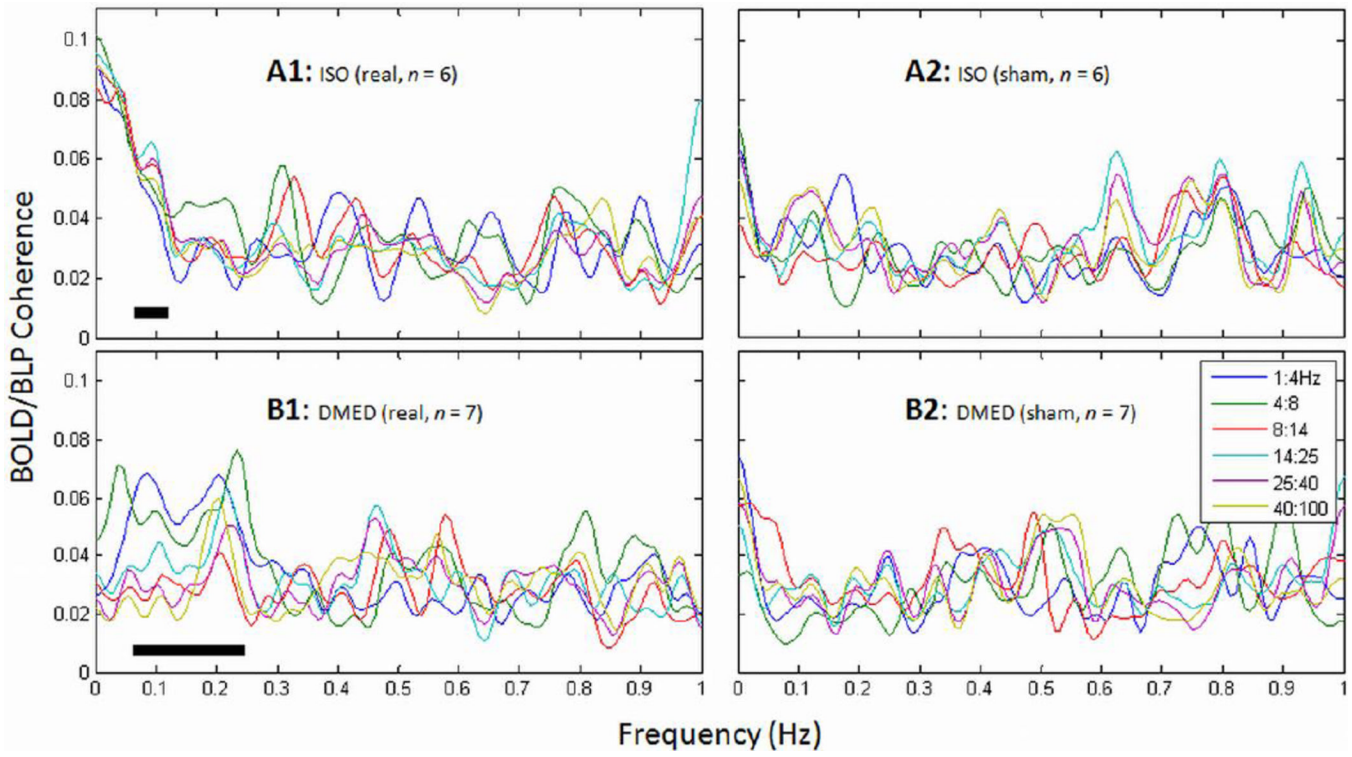

Fig. 4.

Average coherence between BOLD and BLP. The low frequencies (A1: below ~0.1 Hz in ISO; B1: below ~0.25 in DMED) exhibited high average coherence between BOLD signals and power changes of various frequency bands of conventional LFP (BLPs). Broadband BLPs were coherent with BOLD in the ISO group, while in the DMED group, the strongest coherence was in the lower frequency bands. As a control, the time-reversed BOLD signals were used for the coherence analysis, shown in A2 and B2. A paired *t*-test revealed significant difference ($p < 0.05$) between real and sham data for the average of all bands for the peak frequencies (revealed by BOLD/infraslow LFP coherence, indicated with stars in Fig. 3, also indicated above the frequency axis with dark lines).

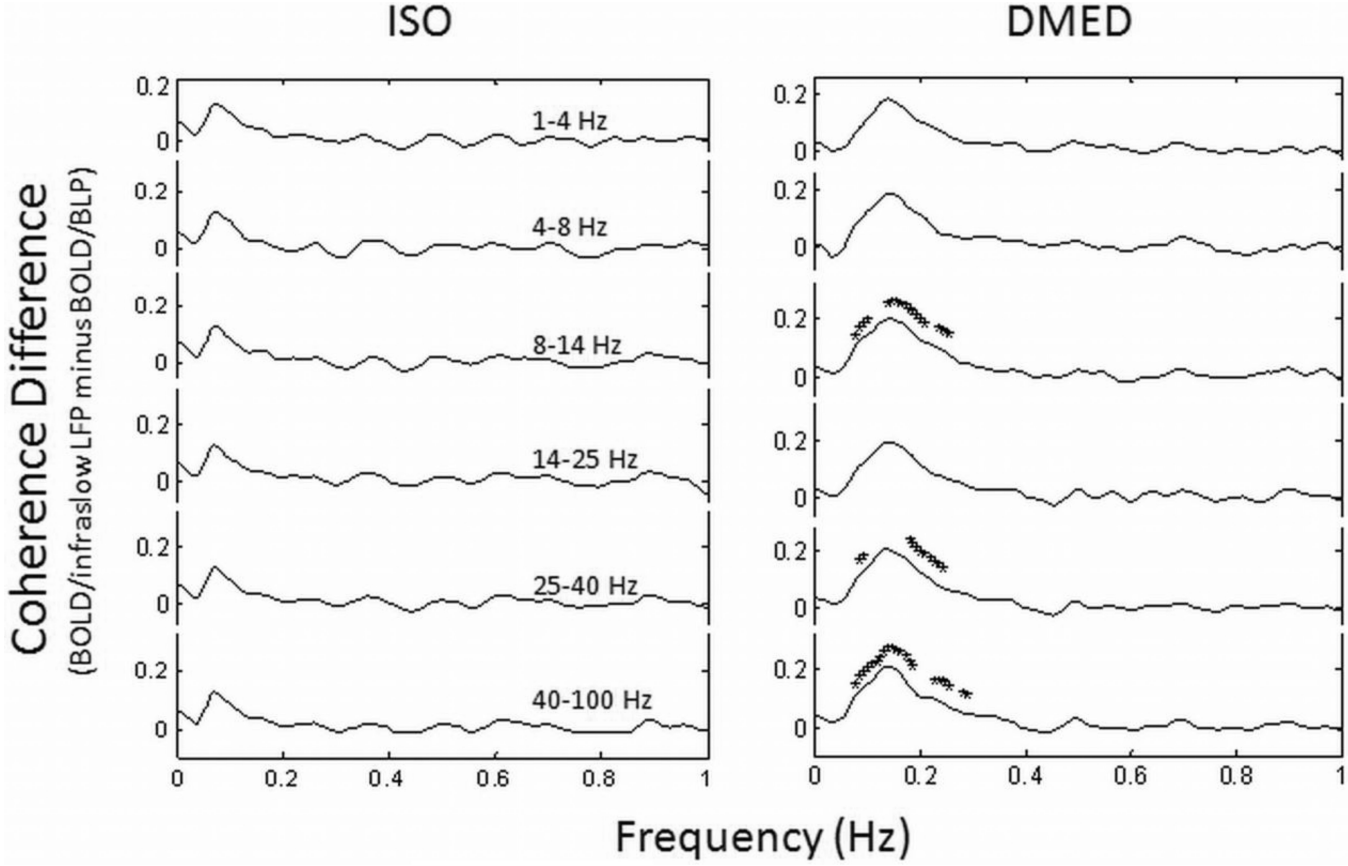

Fig. 5.

Coherence difference between BOLD/infraslow LFP and BOLD/BLP. The differences of average BOLD coherence with infraslow LFP and with BLP of various LFP bands (indicate above the traces) are plotted for the ISO and DMED groups separately. The frequency points with a significant difference ($p < 0.05$, paired t-test, FDR corrected for multiple comparison) are marked with '*'. There are no significant differences between BOLD coherence with infraslow LFP and with BLP in ISO group; some points around 0.1–0.2 Hz in DMED group show significant coherence differences between BOLD/infra slow LFP and BOLD/BLP of the alpha band (4–8 Hz) and the gamma band (> 25 Hz).